Photoionization of radium: Investigating many-body effects at high Z

Mickey Kutzner, Paul Pelley, Lauralea Banks, and Richard Robertson
Department of Physics, Andrews University, Berrien Springs, Michigan 49104-0380
(Received 20 August 1999; published 13 January 2000)

The total and partial photoionization cross sections, branching ratios, and photoelectron angular-distribution asymmetry parameters have been calculated for atomic radium ($Z=88$) for all subshells from the $7s$ valence shell down to the deep $n=3$ subshells. The relativistic random-phase approximation, the relativistic random-phase approximation modified to include relaxation effects, and the relativistic random-phase approximation modified to include relaxation effects and Auger decay were all used to determine the relative importance of various many-body effects such as interchannel coupling, core relaxation, and Auger decay. Comparisons are made between the various theoretical models and experimental data for the total cross sections. Interchannel coupling was found to be important for most subshells. Relaxation effects were found to be significant for calculations of the total cross section above the $5d$ threshold and to have a very large effect on the $5p$ partial photoionization cross section.

PACS number(s): 32.80.Hd, 32.80.Fb

I. INTRODUCTION

The vacuum ultraviolet (VUV) and x-ray absorption spectra of radium ($Z=88$) are important for two reasons: (i) photoionization is an excellent probe of various many-body effects that have not been thoroughly studied in high-Z elements and (ii) the practical necessity of dealing with radioactive waste of uranium processing that contains some radium. Electrons in the deep inner shells of radium have very large effective Z and are thus highly relativistic. It is interesting to determine at what depth of inner shell the electron correlation effects become negligible.

Experimental x-ray absorption spectra at particular characteristic wavelengths have been tabulated for all elements from hydrogen through uranium ($Z=92$) by Henke, Gullikson, and Davis [1]. Theoretical work on radium photoionization has included studies using relativistic Dirac-Slater calculations of the $6p$ subshell [2] and $5d$ subshell [3]; also the closed-shell electron structure of the ground state of radium makes photoionization studies within the relativistic random-phase approximation (RRPA) possible. Deshmukh, Radojević, and Manson [4,5] calculated photoionization cross sections, angular-distribution asymmetry parameters, and branching ratios for outer subshells of both radium and radon using the RRPA. Their radium calculations included interchannel coupling of the 20 relativistic dipole channels from the $7s$ subshell down to the $5p$ subshell. They found many interesting correlation effects in the photoionization parameters due to interchannel coupling including correlation-induced Cooper minima in cross sections and dips in the angular-distribution asymmetry parameters. Recently, Chantler [6] published a compilation of Dirac-Hartree-Fock calculations of photoionization of elements from hydrogen to uranium that complement the experimental work of Henke, Gullikson, and Davis [1].

The importance of including the effects of core relaxation in calculations of inner-shell photoionization in many atomic systems has long been established. Relaxation effects were found to be crucial in calculations of the $4d$ and $3d$ subshells of Xe [7] and Ba [8]. The calculated photoionization cross section of $4f$ electrons from Hg was also found to depend critically on the inclusion of relaxation effects [9].

The purpose of this paper is to study the role of many-body effects, in particular interchannel coupling and core relaxation, on the photoionization parameters in the vicinities of various thresholds. The calculations extend from photon energies just above the valence photoionization threshold to energies capable of ejecting electrons from the very deep $n=3$ shell. The calculations were carried out within the framework of the RRPA, the relativistic random-phase approximation modified to include relaxation (RRPAR), and the relativistic random-phase approximation modified to include relaxation and Auger decay (RRPARA). Where possible, we compare the results of theory with experiments [1] to evaluate the merits of the various approximation techniques. In Sec. II, we review the methods of the RRPAR and RRPARA. The results are reported in Sec. III in a shell-by-shell manner. Section IV is a discussion of some of the implications of this work.

II. METHODS

The RRPA was first introduced in the work of Johnson and co-workers [10]. It is a fully relativistic implementation of the random-phase approximation with exchange (RPAE) developed by Amusia [11]. In the RRPA, the partial photoionization cross section for a particular subshell is given by

$$\sigma_{n\kappa}=\frac{4\pi^2\alpha\omega}{3}(|D_{nj\rightarrow j-1}|^2+|D_{nj\rightarrow j}|^2|D_{nj\rightarrow j+1}|^2), \quad (1)$$

where n is the principal quantum number, ω is the photon energy, and $\kappa=\mp(j+\frac{1}{2})$ for $j=l\pm\frac{1}{2}$, where j and l are the single-electron total and orbital angular-momentum quantum numbers, respectively. The dipole matrix element $D_{nj\rightarrow j'}$ is the reduced RRPA dipole matrix element for the photoionization channel $nj\rightarrow j'$.

The angular-distribution asymmetry parameter $\beta_{n\kappa}$ for the subshell $n\kappa$ is defined in terms of the differential photoionization cross section as

$$\frac{d\sigma_{n\kappa}}{d\Omega}=\frac{\sigma_{n\kappa}(\omega)}{4\pi}\{1-\tfrac{1}{2}\beta_{n\kappa}(\omega)P_2[\cos(\theta)]\} \tag{2}$$

where θ is the angle measured between the directions of the incident photon and the photoelectron. When a subshell is split by spin-orbit splitting into two different levels κ and κ', it is conventional to use the weighted average given by

$$\overline{\beta}=\frac{\sigma_{n\kappa}\beta_{n\kappa}+\sigma_{n\kappa'}\beta_{n\kappa'}}{\sigma_{n\kappa}+\sigma_{n\kappa'}}. \tag{3}$$

The RRPAR method approximates the effects of core relaxation by calculating the continuum photoelectron orbitals in the potential of the relaxed ion. The ionic core with the hole in the level with $j=l+\frac{1}{2}$ has a lower ionization threshold energy and also represents the most populated of the two levels. Thus, we generally consider the hole to be in the subshell with largest j for the purpose of obtaining the V^{N-1} potential. Overlap integrals of the form $\mathrm{Det}\langle\Phi_i'|\Phi_i\rangle$ between orbitals of the unrelaxed ground state Φ_i and the corresponding orbitals of the final relaxed state Φ_i' are included in the RRPAR dipole matrix element for each electron i of the ionic core. Inclusion of these overlap integrals is important for calculation of the partial photoionization cross sections since they approximately remove oscillator strength due to double-excitation shake-up and shake-off processes from the single-excitation channel oscillator strength [12]. In the RRPARA we approximately include the effects of Auger decay by adding to the RRPAR dipole matrix element contributions involving overlap integrals between orbitals of the ground state and the continuum orbitals of the final state.

Photoionization thresholds in the strict RRPA model are the Dirac-Hartree-Fock (DHF) eigenvalues. However, experimental thresholds are frequently utilized. In this work we have used DHF eigenvalues as the threshold for RRPA calculations. The DHF eigenvalues were obtained using the Oxford multiconfiguration Dirac-Fock computer code of Grant *et al.* [13]. In the RRPAR and RRPARA, we have used the difference in total self-consistent field energies of the neutral atom and ion (ΔE_{SCF}) for the threshold energies although experimental threshold energies [14] could also have been used. Table I summarizes the DHF eigenvalues and ΔE_{SCF} energies used for all channels incorporated in the present study along with the experimental threshold energies [14].

The RRPA theory predicts results that are gauge independent provided that one has included all possible dipole-excited channels [10]. In practice, where one limits the number of channels (the truncated RRPA), there will be differences between the ''length'' and ''velocity'' gauge results. Also, the inclusion of relaxation effects in the RRPAR and RRPARA potentials and use of threshold energies other than DHF eigenvalues leads to differences in calculations performed in the two gauges. Results of calculations of cross sections presented in this paper will normally appear as the geometric mean of length and velocity results.

Regions where autoionizing resonances dominate the cross section have not been dealt with here. A combination of RRPA dipole matrix elements and the relativistic multichannel quantum-defect theory (MQDT) could be used to study these complex regions in the absorption spectrum.

TABLE I. Photoionization thresholds (in a.u.) for the various subshells of atomic radium. The second column lists the absolute values of single-particle eigenvalues from a Dirac-Hartree-Fock (DHF) calculation using the code of Ref. [13]. The third column lists the absolute value of the difference between self-consistent field calculations of total energy of the neutral atom and the ion (ΔE_{SCF}). The fourth column lists the experimental threshold energies [14].

Subshell J	DHF	ΔE_{SCF}	Expt.
$7s_{1/2}$	0.166 359	0.160 156	
$6p_{3/2}$	0.740 218	0.691 406	0.691 ± 0.07
$6p_{1/2}$	0.973 599	0.912 109	0.691 ± 0.07
$6s_{1/2}$	1.626 282	1.562 500	1.60 ± 0.08
$5d_{5/2}$	2.901 972	2.740 234	2.47 ± 0.06
$5d_{3/2}$	3.116 783	2.947 266	2.47 ± 0.06
$5p_{3/2}$	6.372 173	6.179 687	5.615 ± 0.07
$5p_{1/2}$	7.843 695	7.626 953	7.365 ± 0.07
$5s_{1/2}$	10.011 71	9.785 156	9.349 ± 0.08
$4f_{7/2}$	11.044 70	10.521 48	10.98 ± 0.09
$4f_{5/2}$	11.354 01	10.818 36	10.98 ± 0.09
$4d_{5/2}$	23.158 27	22.630 86	21.15 ± 0.06
$4d_{3/2}$	24.416 29	23.875 00	23.37 ± 0.06
$4p_{3/2}$	33.395 58	32.861 32	32.31 ± 0.07
$4p_{1/2}$	40.117 70	39.525 39	38.866 ± 0.07
$4s_{1/2}$	45.726 82	45.132 81	44.408 ± 0.06
$3d_{5/2}$	115.952 31	114.632 81	114.10 ± 0.06
$3d_{3/2}$	121.308 30	119.947 27	119.38 ± 0.06
$3p_{3/2}$	141.177 53	139.949 22	139.34 ± 0.06
$3p_{1/2}$	167.244 09	165.908 20	164.98 ± 0.07
$3s_{1/2}$	179.855 53	178.574 22	177.20 ± 0.05

III. RESULTS

A. The 7*s* subshell

The valence shell of radium was previously studied by Deshmukh, Radojević, and Manson [4,5] in the RRPA. The photoionization cross section above the valence threshold in the RRPA and RRPAR approximations are shown in Fig. 1. In this investigation, the 20 coupled relativistic dipole channels, which include all channels originating from subshells $7s$, $6p$, $6s$, $5d$, and $5p$, were employed for the calculation of the $7s$ cross section. The RRPARA is not shown in Fig. 1 since Auger effects are noted only for inner-shell photoionization. The focus of this study is on the near-threshold region. A common effect of relaxation may be seen by a comparison of the RRPA and the RRPAR results of Fig. 1. The rearrangement allowed for in the RRPAR yields a less sharply defined potential for the calculation of the outgoing photoelectron wave function than would be used in a frozen-core calculation. This effectively moves oscillator strength from the discrete transitions below the threshold into the continuum. The location of the Cooper minimum has also been moved to higher energy by the inclusion of rearrange-

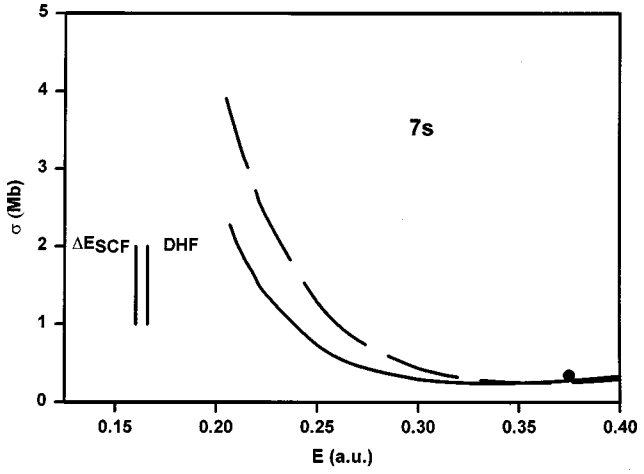

FIG. 1. Photoionization of the $7s$ valence shell of radium. Solid curve is the RRPA and dashed curve is the RRPAR. Dirac-Hartree-Fock (DHF) eigenvalue was used for the RRPA threshold and the difference in total self-consistent field energies of the neutral atom and ion (ΔE_{SCF}) was used for RRPAR calculations. Solid circle represents experimental data from Ref. [1].

ment effects. The only experimental data point [1] lies well above threshold where the unrelaxed calculation is expected to be best.

The accuracy of the RRPAR for the $7s$ valence shell is questionable. The RRPAR assumes the rearrangement has been accomplished only in the final state of the particular subshell under consideration. For valence subshells, the diagrams in many-body perturbation theory representing ground-state correlations make a significant contribution to the correlated dipole matrix element; the lack of inclusion of rearrangement effects in the ground-state correlation (time-reversed) diagrams can unbalance the sometimes delicate balance between final- and ground-state correlation [11]. The importance of ground-state correlations in valence shell photoionization is also reflected in the fact that the ΔE_{SCF} energy does not generally accurately predict the experimental ionization energy for valence shells.

The angular-distribution asymmetry parameter β for the $7s$ valence shell is shown in Fig. 2 in both the RRPA and RRPAR. In the absence of relativistic interactions, the parameter β for an s subshell of a closed-shell atom has the value 2, independent of energy [15]. However, the interaction between the two channels $7s \rightarrow \epsilon p_{1/2}$ and $7s \rightarrow \epsilon p_{3/2}$ in the vicinity of the Cooper minima causes β to fall close to the minimum value of -1. Relaxation effects push the Cooper minimum to higher energies and thus the dips in β are pushed out toward higher energies as well.

B. The $6p$ subshell

The total photoionization cross section above the $6p$ threshold is shown in Fig. 3 for the RRPA and RRPARA. The RRPA (RRPARA) thresholds are denoted DHF (ΔE_{SCF}). The experimental data from Ref. [1] is also shown for comparison. Clearly, relaxation effects play only a very minor role for this subshell. The two experimental data points shown with lowest energy are in excellent agreement

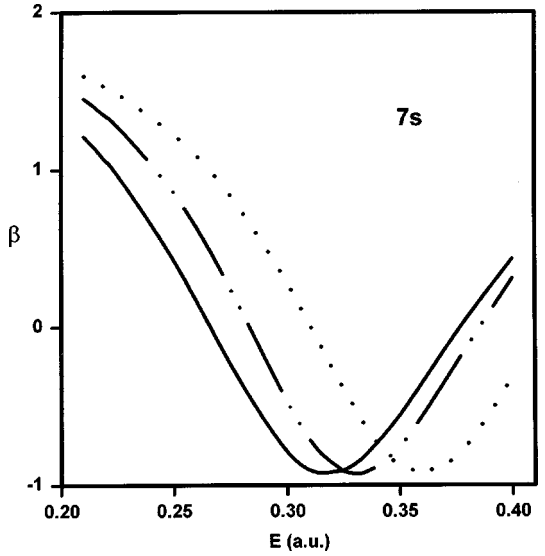

FIG. 2. Photoelectron angular-distribution asymmetry parameter β for $7s$ electrons of atomic radium in the RRPA and RRPAR. Solid line is RRPA, dotted line is RRPAR length, and dashed-double-dot line is RRPAR velocity.

with both the RRPA and RRPARA. The large value of the measured cross section just below 3 a.u. is most probably due to autoionizing resonances below the $5d_{5/2}$ and $5d_{3/2}$ thresholds. The importance of including interchannel coupling is demonstrated by comparison with the Dirac-Hartree-Fock calculation [6], which differs significantly from the RRPA near threshold.

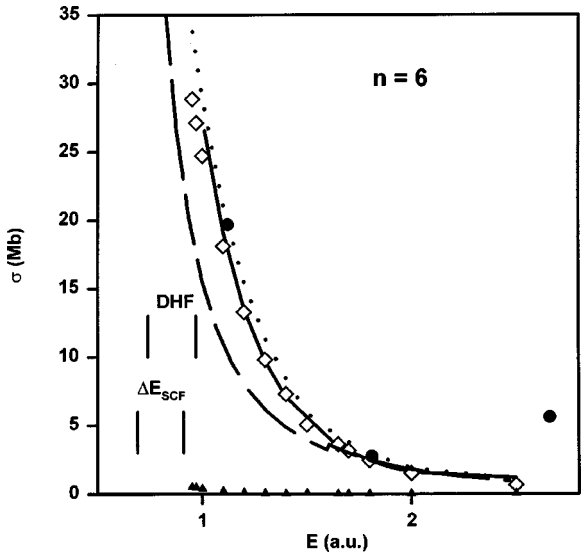

FIG. 3. Photoionization cross sections above the $6p$ threshold of radium. The solid line is the total RRPA cross section, whereas the dotted line is the total RRPARA cross section. RRPAR is not shown but is nearly indistinguishable from the RRPARA. The dashed line is the Dirac-Hartree-Fock calculation of Ref. [6]. Open diamonds and solid triangles are the partial photoionization cross section for direct photoionization of $6p$ and $7s$ electrons, respectively, in the RRPARA. Solid circles are experimental measurements of total absorption from Ref. [1].

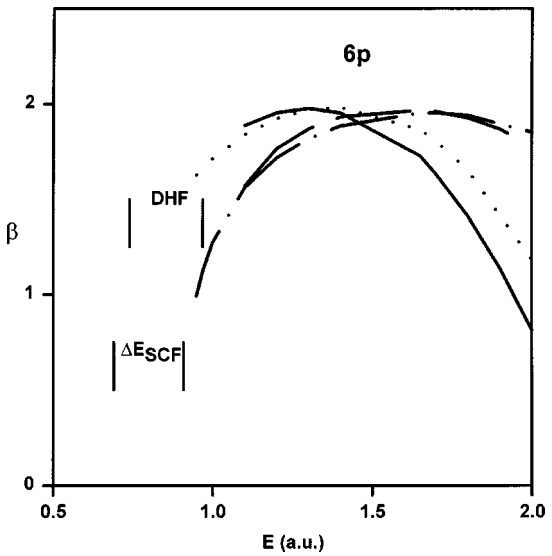

FIG. 4. Photoelectron angular-distribution asymmetry parameter β for $6p$ electrons of radium. The solid and dotted lines are $6p_{3/2}$ in the RRPA and RRPARA, respectively. The dot-dashed and dashed lines are $6p_{1/2}$ in the RRPA and RRPARA, respectively.

Partial photoionization cross sections are also shown for the main-line removal of $6p$ electrons in the RRPARA. In the RRPA, the only difference between the total and partial $6p$ cross section is due to the contributions of the relatively weak $7s$ and $6s$ cross sections. However, in the RRPARA, the partial cross section is also reduced by the overlap integral that reduces the cross section by 12.9%.

Angular-distribution asymmetry parameters for the $6p_{3/2}$ and $6p_{1/2}$ subshells are shown in Fig. 4 in the RRPA and RRPARA. There is quantitatively little difference between the RRPA and RRPARA calculations near threshold.

Another photoionization parameter of interest is the branching ratio $\gamma \equiv \sigma(6p_{3/2})/\sigma(6p_{1/2})$. Shown in Fig. 5, this

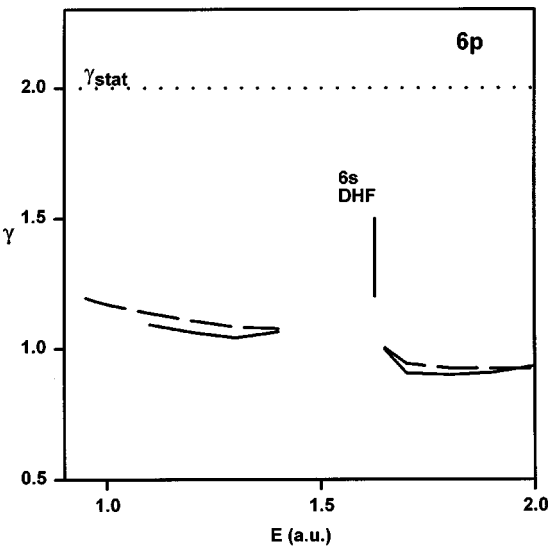

FIG. 5. $6p_{3/2}$:$6p_{1/2}$ branching ratio γ for radium in the RRPA (solid line) and RRPARA (dashed line). The statistical ratio of 2.0 is also shown as a dotted line for comparison.

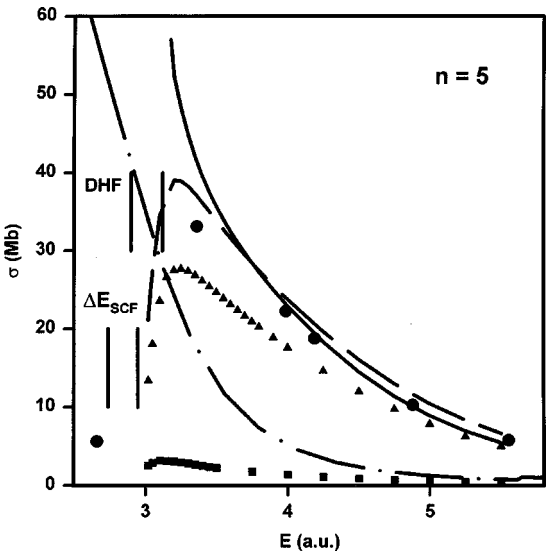

FIG. 6. Photoionization cross sections above the $5d$ threshold of radium. Total cross sections are shown in the RRPA (solid line), RRPARA (dashed line), and Dirac-Hartree-Fock (dot-dash line) from Ref. [6]. The experimental total cross section from Ref. [1] is shown as solid circles. The partial cross section for direct $5d$ photoionization in the RRPARA is shown as triangles and the partial cross section for all other single-excitation channels is shown as squares.

parameter varies significantly from the statistical value based on the ratio of occupation numbers of 2 in this region as reported earlier by Deshmukh, Radojević, and Manson [5]. The branching ratio falls below the value of 2 because both the $6p_{3/2}$ and $6p_{1/2}$ partial cross sections become smaller with increasing energy and the $6p_{3/2}$ begins its decline at a lower threshold energy than does the $6p_{1/2}$. Here again, the relaxation effects are subtle.

C. The $5d$ subshell

It is in the $5d$ subshell that effects of relaxation assume some importance. The total $5d$ photoionization cross section is shown in Fig. 6 in the RRPA and RRPARA along with experimental measurements [1]. The effects of interchannel coupling may be noted by comparing the Dirac-Hartree-Fock calculation [6] with the RRPA. The RRPA and RRPARA calculations in this energy range included 20 relativistic dipole channels from the $7s$ subshell into the $5p$ subshell. Near threshold, the RRPA cross section assumes a very large value dropping monotonically until the $5p$ threshold. The RRPARA (which differs negligibly from RRPAR for this subshell) is small near threshold rising to a peak and then falling off at a slower rate than RRPA until the $5p$ threshold. In the RRPARA, oscillator strength has been shifted from the near-threshold region to higher energies, giving the cross section something of the appearance of a shape resonance as seen in the $4d$ cross sections of Xe, Ba, and lanthanides [7,8]. The Dirac-Hartree-Fock calculation [6] is well below all of the calculations that include interchannel coupling and experiment [1].

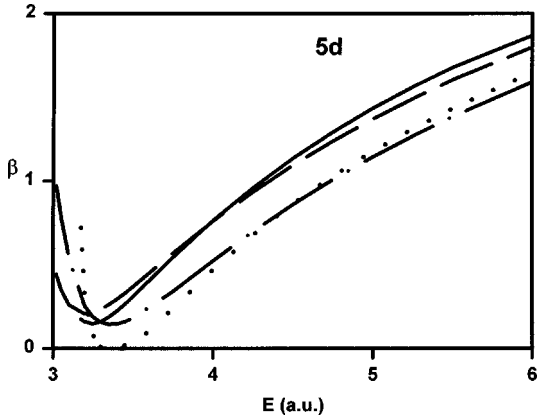

FIG. 7. Photoelectron angular-distribution asymmetry parameter β for $5d$ electrons of radium. The $5d_{5/2}$ is shown as solid line and dashed line for the RRPA and RRPARA, respectively. The $5d_{3/2}$ is shown as dotted and dot-dashed line for the RRPA and RRPARA, respectively.

Also shown in Fig. 6 is the $5d$ partial cross section and the sum of all other single-excitation channels in this energy region in the RRPARA. Since the experimental data represents the total photoionization cross section, it must not be compared with the partial cross sections. Photoelectron spectroscopy could be used to determine the fraction of the total absorption due to direct photoionization of $5d$ electrons. It should also be noted that in the RRPARA, the sum of all of the single-excitation channel cross sections is less than the total cross section since the inclusion of overlap integrals reduces the partial cross sections substantially. The reduction represents oscillator strength due to multiple-excitation channels.

The angular-distribution asymmetry parameter β is less sensitive than the cross section to relaxation effects since it depends on ratios of matrix elements according to the formulation [10,16]

$$\beta_{n\kappa}(\omega)=\left[\frac{1}{2}\frac{(2j-3)}{2j}|D_{j\to j-1}|^2-\frac{3}{2j}\left(\frac{2j-1}{2(2j+2)}\right)^{1/2}\right.$$
$$\times(D_{j\to j-1}D^*_{j\to j}+\text{c.c.})-\frac{(2j-1)(2j+3)}{2j(2j+2)}|D_{j\to j}|^2$$
$$-\frac{3}{2}\left(\frac{(2j-1)(2j+3)}{2j(2j+2)}\right)^{1/2}(D_{j\to j-1}D^*_{j\to j+1}+\text{c.c.})$$
$$+\frac{1}{2}\frac{(2j+5)}{-(2j+2)}|D_{j\to j+1}|^2+\frac{3}{(2j+2)}\left(\frac{2j+3}{2(2j)}\right)^{1/2}$$
$$\left.\times(D_{j\to j}D^*_{j\to j+1}+\text{c.c.})\right](|D_{j\to j-1}|^2+|D_{j\to j}|^2$$
$$+|D_{j\to j+1}|^2)^{-1}. \quad (4)$$

In Fig. 7, β is shown in the RRPA and RRPARA. The substantial changes noted in the $5d$ cross sections due to relaxation effects are not reflected in the β parameter. This has been noted previously in the case of barium and xenon [7].

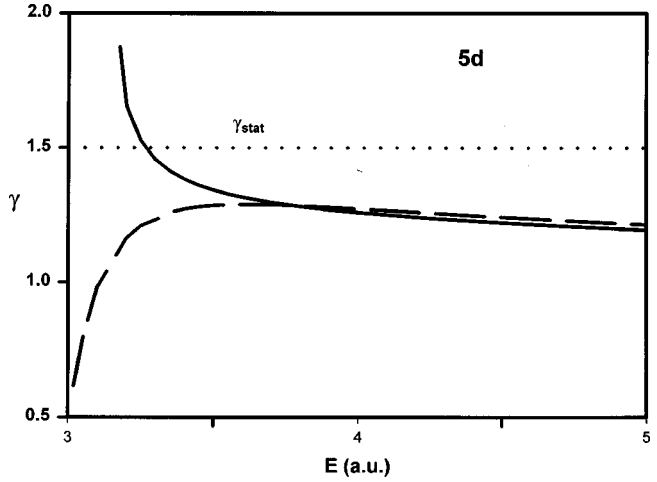

FIG. 8. $5d_{5/2}$:$5d_{3/2}$ branching ratios γ for radium. RRPA is the solid line and the RRPARA is the dashed line. The statistical ratio of 3/2 is also shown for comparison purposes.

Branching ratios $\gamma=\sigma(5d_{5/2})/\sigma(5d_{3/2})$ for the RRPA and RRPARA are shown in Fig. 8 along with the statistical ratio of 3/2. It is interesting to note that near threshold the RRPA predicts a branching ratio above the statistical ratio and the RRPARA predicts a branching ratio below the statistical ratio. The RRPA and RRPARA eventually agree with one another at approximately 1 a.u. above the threshold.

D. The $5p$ subshell

The $5p$ subshell is interesting because of large interchannel coupling effects as well as very large relaxation effects. Figure 9 shows the total photoionization cross sections as well as the partial $5p$ cross sections in the RRPA, RRPARA in the vicinity of the $5p$ thresholds. The experimental data [1] is the total photoionization cross section. The spin-orbit splitting is very large for this subshell. Again, for this subshell, the Dirac-Hartree-Fock calculation is well below the

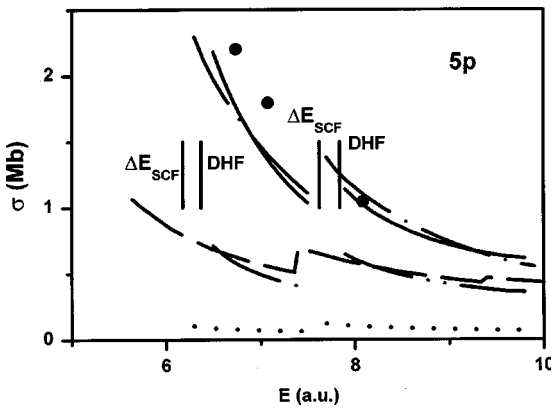

FIG. 9. Photoionization cross sections near the $5p$ thresholds of radium. Total cross sections are shown for the RRPA (solid line), RRPARA (dot-dashed line), Dirac-Hartree-Fock from Ref. [6] (dashed line) and experiment from Ref. [1] (solid circles). Partial $5p$ cross sections are shown for the RRPA (double-dot dashed line) and RRPARA (dotted line).

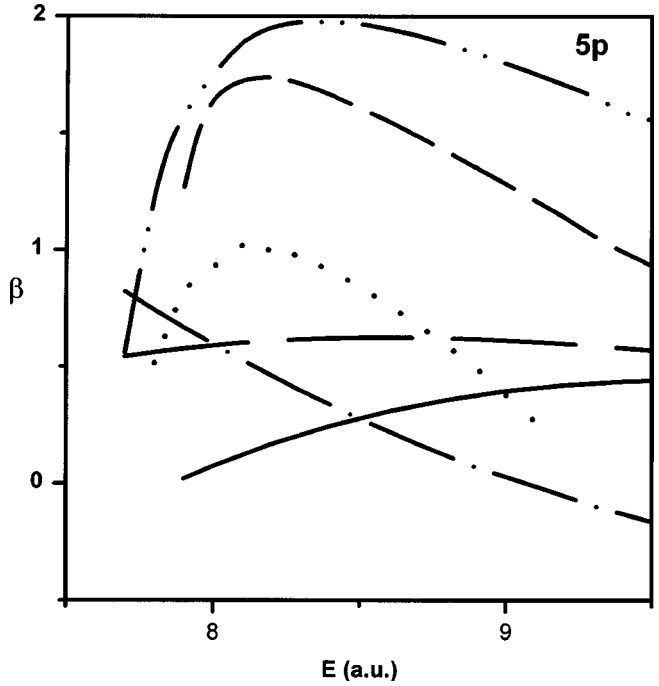

FIG. 10. Photoelectron angular-distribution asymmetry parameters β for $5p$ electrons of radium. For $5p_{3/2}$ electrons, the solid line is the RRPA, the long-dashed line is the RRPAR, the dot-dashed line is the RRPARA. For $5p_{1/2}$ electrons, the short-dashed line is the RRPA, the dotted line is the RRPAR, and the dashed double-dot line is the RRPARA.

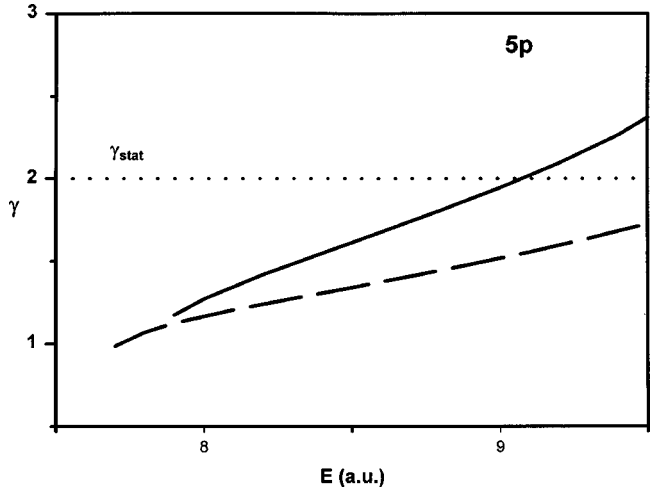

FIG. 11. $5p_{3/2}$:$5p_{1/2}$ branching ratio γ for radium. The solid line is the RRPA and the dashed line is the RRPARA.

calculations that include interchannel coupling and the experiment [1]. The total photoionization cross section in this region is still dominated by the $5d$ channels so that the inclusion of relaxation effects does not alter the total photoionization cross section greatly. However, the removal of the $5p$ electron causes dramatic rearrangement of the $7s$, $6p$, and to a lesser extent the $5d$ electronic orbitals. The reduction of the $5p$ single-excitation channel cross sections due to overlap integrals is approximately 79%. This oscillator strength is redistributed to multiple-excitation processes. A comparison of the $5p$ partial cross sections in the RRPA and RRPARA in Fig. 9 shows the large effect of rearrangement.

In Fig. 10, the angular-distribution asymmetry parameters β for the $5p$ subshell are presented in the RRPA, RRPAR, and RRPARA. The RRPA results presented here are very different than those presented by Deshmukh, Radojević, and Manson [5], because we have included the 19 dipole-allowed channels derived from channels originating from $5d$, $5p$, $5s$, and $4f$ subshells, where Deshmukh, Radojević, and Manson [5] included the 20 channels originating from $7s$, $6p$, $6s$, $5d$, and $5p$ subshells. Evidently, the interactions between the $5p$ subshell channels and the $4f$ subshell channels are important. Relaxation effects are also seen to be large for the $5p$ subshell β parameters, particularly for the $5p_{3/2}$ subshell where the slope of the RRPARA calculation is of opposite sign than the slope of the RRPA calculation.

The branching ratio $\gamma=\sigma(5p_{3/2})/\sigma(5p_{1/2})$ shown in Fig. 11 appears to be somewhat less sensitive to relaxation effects than either the cross section or the β parameter. The RRPA and RRPARA branching ratios are in agreement near threshold where relaxation effects should be most apparent. It is interesting to again note that the RRPA result reported here is considerably larger above 9 a.u. than the result reported in Ref. [5] because of the inclusion here of interchannel coupling with the $4f$ channels.

E. The $4f$ subshell

The $4f$ subshell of radium has previously been studied only in Dirac-Hartree-Fock calculations [6]. In the case of atomic mercury, it was found that relaxation effects had a large influence on the $4f$ photoionization cross section [9]. For radium, however, the effective Z for $4f$ electrons is considerably larger than it was for mercury, lessening the importance of relaxation effects. The total photoionization cross sections in the energy region where $n=4$ subshell cross sections dominate the absorption are shown in Fig. 12 in the RRPA and RRPARA. The initial rise in the cross section is due to $4f$ photoionization with the centripetal barrier causing a delay of the onset of absorption. The absorption of $4d$ and $4p$ electrons causes the double peaks in the cross section between 20 and 40 a.u., respectively, with $4s$ absorption leading to a slight change in the second derivative of the cross section between 40 and 60 a.u. It should be noted that good agreement between theory and experiment throughout the entire energy range was achieved only when interchannel coupling between the $n=5$ and $n=4$ channels was included. The results shown in Fig. 12 included 30 relativistic dipole channels originating from $5d$, $5p$, $4f$, $4d$, $4p$, and $4s$ subshell electrons. For comparison purposes, the Dirac-Hartree-Fock calculations of Chantler [6] are also shown. Although the shape of the Dirac-Hartree-Fock calculation is not very different from the calculations including interchannel coupling, the overall scale is considerably different. Relaxation effects are not large on the total cross section, however, the partial $4f$ cross sections are reduced by 22.3% due to the inclusion of overlap integrals. The $4f$ angular-distribution

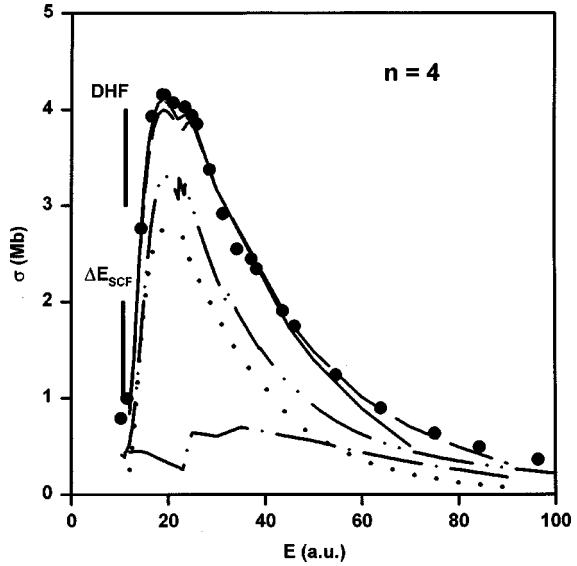

FIG. 12. Photoionization cross sections above the $4f$ threshold of radium. Total cross sections are shown in the RRPA (solid line), RRPARA (dashed line), Dirac-Hartree-Fock from Ref. [6] (double-dot dashed line) and experiment from Ref. [1] (solid circles). The dotted line is the partial photoionization cross section of $4f$ electrons alone in the RRPARA. The dot-dashed line is the sum of the photoionization cross sections from all other single-excitation channels.

asymmetry parameter and branching ratio shown in Figs. 13 and 14, respectively, are also not greatly influenced by relaxation effects.

F. The $3d$ subshell

In this extremely deep inner subshell, most of the many-electron correlation effects might be thought to be small compared with the overriding influence of the nucleus. The total photoionization cross sections above the $3d$ threshold are shown in Fig. 15 for the RRPA, the RRPAR, and the RRPARA. The calculations included 32 relativistic dipole-allowed channels including excitations of $4f$, $4d$, $4p$, $4s$, $3d$, $3p$, and $3s$ electrons. Near-threshold, relaxation effects reduce the cross section as seen in the RRPAR. However, accounting for downward transitions of $4f$ electrons into the $3d$ vacancy in the RRPARA tends to nearly restore the total

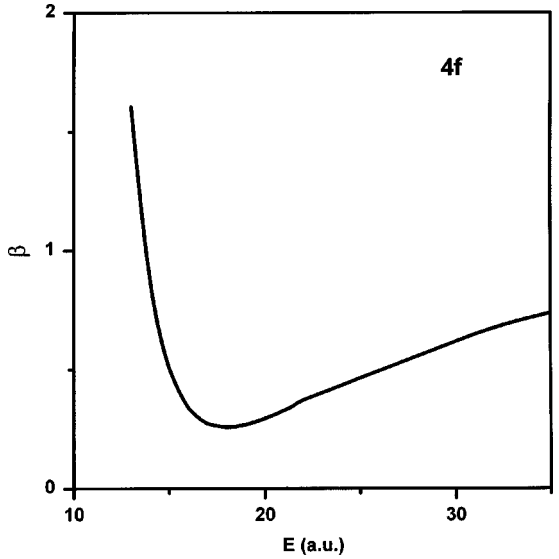

FIG. 13. Photoelectron angular-distribution asymmetry parameters β for $4f$ electrons of radium. Plots are nearly indistinguishable for $4f_{7/2}$ and $4f_{5/2}$ electrons. RRPA and RRPARA predict nearly identical results.

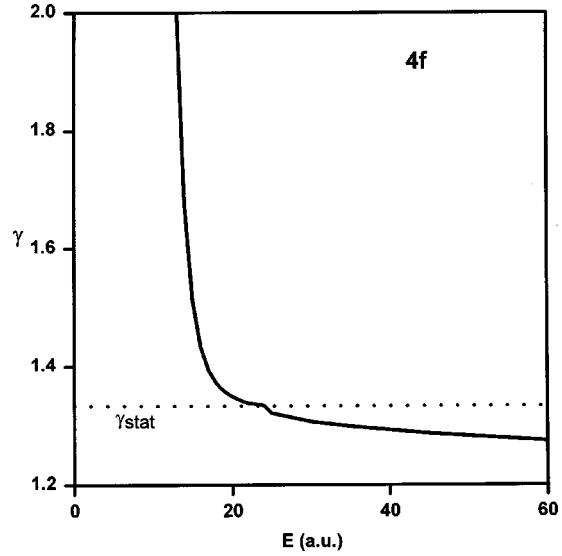

FIG. 14. $4f_{7/2}$:$4f_{5/2}$ branching ratio γ for radium in the RRPA. RRPARA prediction is nearly indistinguishable from the RRPA. The statistical ratio of 4/3 is also shown for comparison.

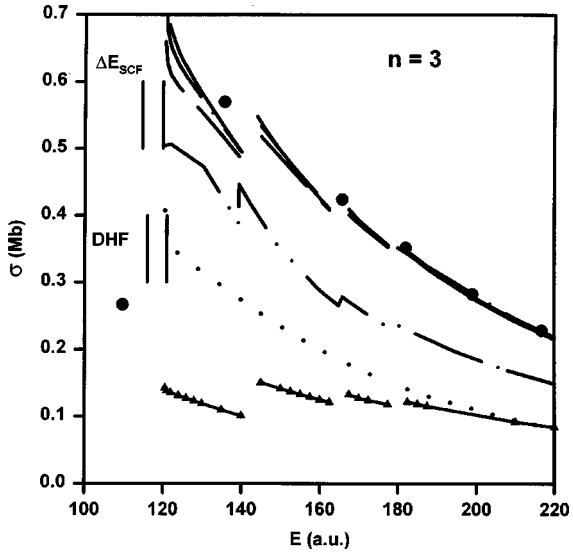

FIG. 15. Photoionization cross sections above the $3d$ thresholds of radium. Total cross sections are shown for the RRPA (solid line), RRPAR (dashed line), and RRPARA (dot-dashed line), Dirac-Hartree-Fock from Ref. [6] (double-dot dashed line) and experiment from Ref. [1] (solid circles). The partial cross section for direct photoionization of $3d$ electrons is shown in the RRPARA as a dotted line. The summed partial cross sections for all other single-excitation channels are shown as a line with solid triangles.

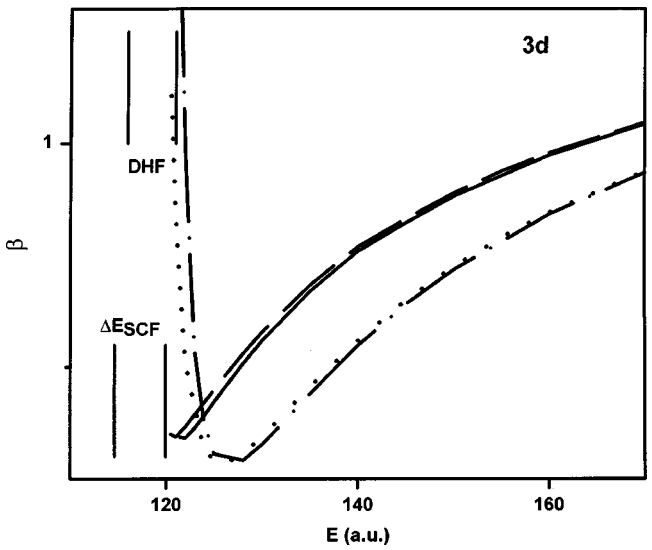

FIG. 16. Photoelectron angular-distribution asymmetry parameter β for $3d$ electrons of radium. For $3d_{5/2}$ electrons, results are shown in the RRPA (solid line) and RRPARA (dashed line). For $3d_{3/2}$ electrons, results are also shown for the RRPA (dot-dashed line) and RRPARA (dotted line).

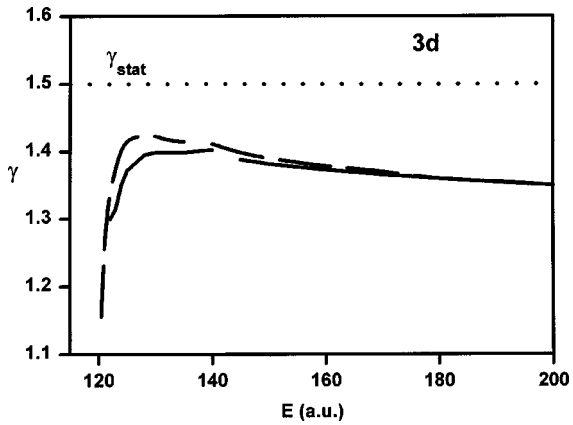

FIG. 17. $3d_{5/2}$:$3d_{3/2}$ branching ratio γ for radium. RRPA is shown by a solid line and RRPARA is shown by the dashed line. The statistical ratio of 3/2 is also shown.

cross section to the RRPA prediction. The Dirac-Hartree-Fock calculations of Chantler [6] are shown for the sake of comparison and are again found to be low. Agreement between the RRPA and experiment [1] is very good, especially at higher energies. Figures 16 and 17 show the angular-distribution asymmetry parameters and the branching ratios for the $3d$ subshell. As was noted for the total photoionization cross section, only subtle differences are detected between the models that include relaxation and those that do not for both β and γ.

IV. CONCLUSION

Relaxation effects and interchannel coupling have been evaluated for photoionization parameters of the various subshells of radium. Relaxation effects are small for the valence and penultimate subshells and the highly correlated RRPA seems to provide an excellent description of the total absorption. However, the $5d$ and $5p$ subshell photoionization parameters seem to be strongly influenced by relaxation effects. The rearrangement of electron orbitals of the ion upon removal of $5p$ electrons is substantial. Interchannel coupling is seen to be important for the angular-distribution asymmetry parameter and branching ratio of the $5p$ subshell. The $4f$ and $3d$ subshell cross sections are only weakly affected by relaxation effects, but interchannel coupling played an important role in obtaining an accurate description of the total photoionization cross sections in the near-threshold regions of both of these deep inner subshells.

It appears that relaxation effects are small for outer subshells where most of the spectator electrons remaining in the ion make only slight adjustments to their orbitals when the photoelectron is removed. The relaxation effects increase as deeper subshells are considered until at deep enough subshells, the nuclear potential dominates and relaxation effects again become small.

It is hoped that the theoretical work presented here will stimulate additional theoretical and experimental work on radium and other high-Z atoms. In particular, resonance regions could be studied both theoretically and experimentally. The new synchrotron light sources could be used to yield absorption spectra with more detail near each of the thresholds where many-body effects are important. Photoelectron spectroscopy could be used to determine branching ratios and partial cross sections. Perhaps even deeper, more highly relativistic inner subshells could be carefully studied with hard x rays and theory.

ACKNOWLEDGMENTS

The authors wish to thank V. Radojević for use of the RRPAR code and Walter Johnson for use of the RRPA code. We also acknowledge Stephen E. Vance and Quinn Shamblin for their role in the development of the RRPARA model. This work has been supported in part by Grant No. PHY-9707183 of the National Science Foundation and by the Office of Scholarly Research of Andrews University.

[1] B. L. Henke, E. M. Gullikson, and J. C. Davis, At. Data Nucl. Data Tables **54**, 181 (1993).
[2] S. T. Manson, C. J. Lee, R. H. Pratt, I. B. Goldberg, B. R. Tambe, and A. Ron, Phys. Rev. A **28**, 2885 (1983).
[3] B. R. Tambe and S. T. Manson, Phys. Rev. A **30**, 256 (1984).
[4] P. C. Deshmukh, V. Radojević, and S. T. Manson, Phys. Rev. A **34**, 5162 (1986).
[5] P. C. Deshmukh, V. Radojević, and S. T. Manson, Phys. Rev. A **45**, 6339 (1992).
[6] C. T. Chantler, J. Phys. Chem. Ref. Data **24**, 71 (1995).
[7] Z. Altun, M. Kutzner, and H. P. Kelly, Phys. Rev. A **37**, 4671 (1988).

[8] V. Radojević, M. Kutzner, and H. P. Kelly, Phys. Rev. A **40**, 727 (1989); M. Kutzner, D. Winn, and S. Mattingly, *ibid.* **48**, 404 (1993).
[9] M. Kutzner, C. Tidwell, S. E. Vance, and V. Radojević, Phys. Rev. A **49**, 300 (1994).
[10] W. R. Johnson and C. D. Lin, Phys. Rev. A **20**, 964 (1979); W. R. Johnson, C. D. Lin, K. T. Cheng, and C. M. Lee, Phys. Scr. **21**, 403 (1980).
[11] M. Ya. Amusia, in *Atomic Photoeffect*, edited by P. G. Burke and H. Kleinpoppen (Plenum, New York, 1990).
[12] T. Åberg, in *Photoionization and Other Probes of Many-Electron Interactions*, edited by F. Wuilleumier (Plenum, New York, 1976).
[13] I. P. Grant, B. J. McKenzie, P. H. Norrington, D. F. Mayers, and N. C. Pyper, Comput. Phys. Commun. **21**, 207 (1980).
[14] J. A. Bearden and A. F. Burr, Rev. Mod. Phys. **39**, 125 (1967).
[15] S. T. Manson and A. F. Starace, Rev. Mod. Phys. **54**, 389 (1982), and references therein.
[16] T. E. H. Walker and J. T. Waber, J. Phys. B **7**, 674 (1974).